Chinese Journal of Aeronautics, (2024), 37(8): 358–372

Chinese Society of Aeronautics and Astronautics
& Beihang University

Chinese Journal of Aeronautics

cja@buaa.edu.cn
www.sciencedirect.com

FULL LENGTH ARTICLE

Game theory based finite-time formation control using artificial potentials for tethered space net robot

Yifeng MA [a], Yizhai ZHANG [a], Panfeng HUANG [a], Ya LIU [b], Fan ZHANG [a,*]

[a] The Research Center for Intelligent Robotics, School of Astronautics, Northwestern Polytechnical University, Xi'an 710072, China
[b] School of Electronic Information and Electrical Engineering, Shanghai Jiao Tong University, Shanghai 200240, China

Received 6 September 2023; revised 11 October 2023; accepted 14 December 2023
Available online 13 April 2024

KEYWORDS

Game theory;
Formation control;
Artificial potential field;
Relative distance constraint;
Tethered space net robot (TSNR)

Abstract The Tethered Space Net Robot (TSNR) is an innovative solution for active space debris capture and removal. Its large envelope and simple capture method make it an attractive option for this task. However, capturing maneuverable debris with the flexible and elastic underactuated net poses significant challenges. To address this, a novel formation control method for the TSNR is proposed through the integration of differential game theory and robust adaptive control in this paper. Specifically, the trajectory of the TSNR is obtained through the solution of a real-time feedback pursuit-evasion game with a dynamic target, where the primary condition is to ensure the stability of the TSNR. Furthermore, to minimize tracking errors and maintain a specific configuration, a robust adaptive formation control scheme with Artificial Potential Field (APF) based on a Finite-Time Convergent Extended State Observer (FTCESO) is investigated. The proposed control method has a key advantage in suppressing complex oscillations by a new adaptive law, thus precisely maintaining the configuration. Finally, numerical simulations are performed to demonstrate the effectiveness of the proposed scheme.

1. Introduction

On-orbit services, such as debris removal and non-cooperative target capture, are promising trends for future space development.[1] To accomplish capture missions, flexible tethered space systems have been proposed in the last few decades. These systems, such as the Tethered Space Net (TSN),[2] Tethered Space Robot (TSR),[3] Tethered Space Net Robot (TSNR),[4,5] and others,[6] connect the capturing device and target with a flexible tether. The TSNR system, shown in Fig. 1, includes a platform satellite, a main connection tether, a connecting net, and four

* Corresponding author.
E-mail address: fzhang@nwpu.edu.cn (F. ZHANG).

Peer review under responsibility of Editorial Committee of CJA.

ELSEVIER Production and hosting by Elsevier

https://doi.org/10.1016/j.cja.2024.04.011

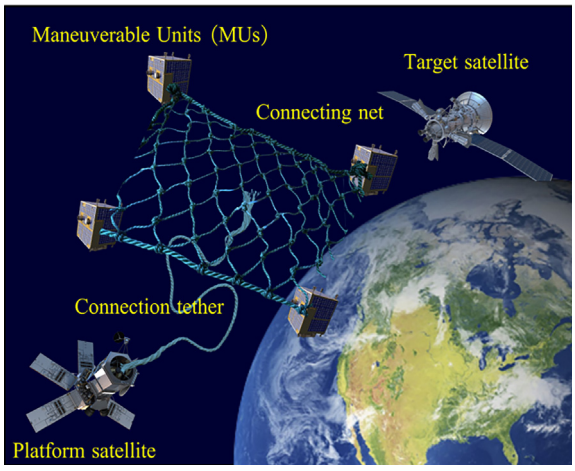

Fig. 1 TSNR system.

corner Maneuverable Units (MUs), which are mostly used for active debris capture and removal.

The TSNR's capture mission consists of four phases: releasing, approaching, capturing, and deorbiting. During the approaching phase, the distances between the MUs are kept very close so that the relative distance constraint must be satisfied.[4] To prevent the flexible net from tangling and the MUs from colliding, a minimal separation distance must be set. A maximal separation distance is also needed to avoid the bouncing effect,[7] which occurs when the aggressive elasticity of the braid tether induces periodical transitions from slack to taut and back to slack.

In recent years, researchers have extensively investigated the control problems of the TSNR with relative constraints. For instance, the work in Ref. 8 designed formation-keeping control strategies using two artificial potential functions to maintain the TSNR's configuration while satisfying the relative distance constraint. In Ref. 9, a fuzzy-based adaptive super-twisting sliding mode control was proposed to estimate and suppress the complex oscillations of the TSNR. Liu et al.[10] designed a continuous fixed-time consensus tracking controller for the TSNR, considering the synchronization of the MUs. The proposed control scheme can eliminate the chattering phenomenon while ensuring convergence precision.

However, in previous work, the relative distance between the TSNR and the target was excessively short. As a result, the desired trajectory of the TSNR was simply determined as a set of regular constant lines, without considering the target's potential maneuvers to evade capture. Furthermore, a suitable control scheme under such maneuvering generated by a probable pursuit-evasion game should be further studied. Therefore, obtaining the short-distance interception trajectory requires modeling the problem as a pursuit-evasion differential game between two competitors, which is often used in many studies. Ye et al.[11] proposed a time-to-go estimation algorithm based on zero effort miss for interception guidance strategies for spacecrafts. The terminal interception time was calculated by recursion. In Ref. 12, the game was converted into a two-point boundary value problem by considering different thruster configurations of the pursuer and the evader, and was solved by combining the heuristic searching and Newton method. Liang et al.[13] addressed game named TAD with three players, including target, attacker, and defender. Based on a barrier, the winning regions of players were obtained, and the optimal strategies were identified and analyzed. In addition, a guidance problem in a two-on-two engagement with a protector joining is investigated in Ref. 14. Two classes of guidance schemes for spacecraft, based on norm differential game and linear quadratic differential game strategies respectively, were proposed. Furthermore, Chao et al.[15] categorized the game process into four phases, C1-C4, based on the switching time. To minimize fuel cost in the C1 and C3, a linear quadratic differential game guidance scheme is utilized. And a norm-bounded game guidance strategy is employed in the C2 and C4 phases to satisfy the constraint of the control input.

Nonetheless, the traditional game scenarios are not suitable for the TSNR, since its planning margin is quite narrow, owing to the relative distance constraints between the MUs which are more restrictive than communication distance limitations. Furthermore, a minor tracking error can cause significant effects on the system during practical capture missions. Therefore, it is crucial to develop a control algorithm that ensures tracking accuracy and reduces the impact of disturbances on the constraints and configuration. Finite-time formation control has a great advantage for this problem, being able to limit the convergence time to a small amount. By using the homogeneity theory, there are many effective methods for finite-time consensus for leader-following multi-agent systems proposed in Refs. 16–18. With the strong robust and high-speed tracking property of Sliding-Mode Control (SMC), the finite-time cooperative tracking problem has also been investigated in Ref. 19 for high-order multi-agent systems.

Nevertheless, the aforementioned studies do not consider maneuvering targets or stringent formation constraints. In this paper, a formation control mechanism is introduced for the TSNR to track the desired trajectory obtained through the application of a pursuit-evasion game. This mechanism incorporates uncertainty perturbation compensation and relative distance constraint assurance. The Finite-Time Convergent Extended State Observer (FTCESO) has been extensively applied as an essential method for estimating system states and compensating for uncertainty disturbances due to its finite-time convergence and lack of peak phenomenon. This method has been previously utilized by Refs. 20,21. Furthermore, the APF method has been widely utilized in formation control problems that require collision avoidance, as shown by Refs. 22,23. Li et al.[24] developed an improved APF method for the follower-satellite that ensures the maintenance of a collision-avoidance relative distance from the corresponding leader-satellite within the desired communication range. In addition, similar work has been conducted by Wang,[25] Wu,[26] and Xu,[27] where they introduced the APF for satellite clusters to achieve the desired formation pattern and collision avoidance. Moreover, utilizing the APF, multiple innovative path-planning schemes have been created for collision-free autonomous vehicles, as demonstrated in Refs. 28,29. Nonetheless, it is worth noting that the derivative of the gradient of the APF can cause violent oscillations, which negatively affect the effectiveness of the controller.

This paper focuses on addressing trajectory planning and configuration maintenance for the constrained TSNR during dynamic target capturing. A novel game theory based formation control scheme is proposed in this paper. The main contributions can be summarized as follows:

(1) Unlike previous studies that focused on static targets and regular constant trajectories,[8–10] this paper presents trajectories for the MUs obtained through the solution of a pursuit-evasion game with a dynamic target.
(2) The pursuit-evasion game incorporates real-time feedback, ensuring that the generated trajectories satisfy the constraint of configurational stability.
(3) A robust adaptive controller is proposed that effectively suppresses tracking errors and ensures compliance with relative distance constraints using the FTCESO and the APF.
(4) To accurately maintain the TSNR configuration, a novel adaptive law is developed to effectively suppress vibrations.

The remainders are stated as follows. Section 2 presents the mission of the TSNR and formulates the control problem. In Section 3, a novel formation control strategy is proposed, and its stability is analyzed. In Section 4, the proposed scheme is validated using numerical simulations and results. Section 5 concludes this paper.

2. Problem formulation

2.1. Mission description

This paper focuses on the approaching phase of the TSNR capture mission, which involves a dynamic target that can evade capture. Initially, the TSNR is stored in the platform satellite. Once the target is detected, the TSNR is ejected and passively unfolded. During the approaching phase, the TSNR attempts to approach the target with an easy-capture pattern, while the target seeks to evade by maximizing the relative distance. To achieve this, a trajectory based on game theory is generated for the TSNR, and a formation control mechanism is developed to ensure trajectory tracking accuracy and configuration maintenance. Assume that the two spacecraft in the pursuit-evasion game with complete information, i.e., both the TSNR and the target know each other's cost functions and control strategies, and relative information is given by the visual navigation sensors on the MUs.

2.2. Dynamics modeling

To describe the orbit movements of the TSNR and the target, the following coordinate frames are depicted in Fig. 2. The Earth-Centered Inertial (ECI) frame, denoted by $EXYZ$, is located at the center of the Earth. The non-inertial Local Vertical Local Horizontal (LVLH) orbit coordinate frame, denoted by $Oxyz$, is located at the platform satellite. The TSNR only undergoes translation relative to the platform satellite, and the relative distance is much smaller than the orbital radius. Furthermore, the TSNR undergoes no rotational motion relative to the platform satellite. The body-fixed frame, denoted by $O_b x_b y_b z_b$ and located at the center of the TSNR, is parallel to the orbital coordinate frame.

A full description of the TSNR has been provided in Ref. 4 (Section 3, Eqs. (1)–(10)). It includes the mechanical design of the net and the four MUs, as well as the derivation of dynamics equations, which can be expressed as follows:

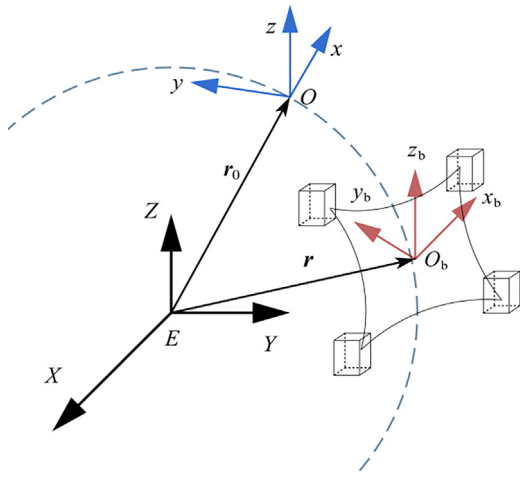

Fig. 2 Coordinate of TSNR system.

$$\begin{cases} \dot{\boldsymbol{x}}_i = \boldsymbol{v}_i \\ \dot{\boldsymbol{v}}_i = \boldsymbol{f}_i(\boldsymbol{x}_i, \boldsymbol{v}_i) + \boldsymbol{u}_i + \boldsymbol{d}_i \end{cases} \tag{1}$$

where $\boldsymbol{x}_i$ denotes the relative position of the i-th MU in the orbital frame, with $i = \mathrm{Aa}, \mathrm{Ak}, \mathrm{Ka}, \mathrm{Kk}$;[9] $\boldsymbol{v}_i$ represents the relative velocity, and $\boldsymbol{u}_i$ denotes the control force; $\boldsymbol{f}_i$ is the dynamic function; $\boldsymbol{d}_i$ is the disturbance on the i-th MU caused by the uncontrollable net and the orbital environment, which is bounded.

During the approaching phase, the relative distance between the adjacent MUs needs to be restricted to avoid snapping elasticity and collision. This can be achieved through the use of relative constraints:

$$\Theta = \{\ell_0 < \| \boldsymbol{x}_i - \boldsymbol{x}_j \| < L_{ij} + \delta, \text{ for } i = 1, 2, \cdots, N, \text{ and } j \in \Omega_i\} \tag{2}$$

where $\| \cdot \|$ denotes the Euclidean norm, ℓ_0 is the minimum safety distance between the MUs, L_{ij} is the side length of the net, δ is the maximum elastic elongation of the net side, N is the number of the MUs, and Ω_i is the set of indices corresponding to the information neighbors of the i-th MU.

Remark 1. In this mission, the TSNR comprises one virtual leader and four followers, where the leader obtains the desired trajectory by solving the pursuit-evasion game with a target, and followers refer to the four MUs. The virtual leader is located at the center of the four MUs. In addition to ensuring relative distance constraints Eq. (2) while tracking the trajectories, the MUs need to maintain a specific configuration, which will be obtained in Section 3.

2.3. Some lemmas

Lemma 1. [24] If k_i is a positive number, and $\boldsymbol{K}$ is a diagonal matrix composed of k_i, then the following relationships exists:

$$\sum_{i=1}^{N} \boldsymbol{x}_i^{\mathrm{T}} k_i \boldsymbol{x}_i^{\gamma} \geqslant \lambda_{\min}(\boldsymbol{K}) \sum_{i=1}^{N} \left(\boldsymbol{x}_i^{\mathrm{T}} \boldsymbol{x}_i\right)^{(\gamma+1)/2} \tag{3}$$

where $\lambda_{\min}(\boldsymbol{K})$ represents the minimum eigenvalue of the gain matrix $\boldsymbol{K}$; γ and N are positive constants.

Lemma 2. [30] Consider a nonlinear system $\dot{x} = f(x)$. Suppose there is a continuous positive Lyapunov function $V(x)$, and real constants $\alpha > 0$, $\beta > 0$, and $0 < \gamma < 1$. If $V(x)$ satisfies the following inequality:

$$\dot{V}(x) + \alpha V(x) + \beta V^{\gamma}(x) \leqslant 0 \tag{4}$$

then the system is globally fast finite-time stable, and the convergence time T_{f}, depending on the initial state $x(0) = x_0$, can be obtained as:

$$T_{\mathrm{f}} \leqslant t_0 + \frac{1}{\alpha(1-\gamma)} \ln \frac{\alpha V^{1-\gamma}(x_0) + \beta}{\beta} \tag{5}$$

where t_0 is the initial time.

3. Controller design

A novel game theory based formation controller (as shown in Fig. 3) is proposed in this section, including two parts: trajectory planning and configuration maintenance. After obtaining the desired trajectory by pursuit-evasion game, each MU tracks its respective trajectory. Additionally, tracking errors and various disturbances are approximated by FTCESO. Furthermore, the APF method is employed to ensure collision-free flight and maintain the required formation pattern, including relative distance constraints. Moreover, the adaptive law in the formation controller compensates for the disturbance and the derivative of the gradient of the APF.

3.1. Pursuit-evasion game generated trajectory

When the target is maneuvering, the TSNR needs to constantly plan its trajectory to catch up with the target while maintaining its configuration. A real-time feedback pursuit-evasion game is proposed to achieve this purpose. The initial state of the virtual leader is located at the center of the MUs. Set the leader and the target respectively as the pursuer and evader in the pursuit-evasion game. For simplicity, only a linear model without disturbance is considered for trajectory optimization. Thus, the relative dynamics Eq. (1) of the two players can be deduced as:

$$\begin{cases} \dot{\boldsymbol{\rho}}_{\mathrm{p}} = \boldsymbol{A}_{\mathrm{p}}\boldsymbol{\rho}_{\mathrm{p}} + \boldsymbol{B}_{\mathrm{p}}\boldsymbol{u}_{\mathrm{p}} \\ \dot{\boldsymbol{\rho}}_{\mathrm{e}} = \boldsymbol{A}_{\mathrm{e}}\boldsymbol{\rho}_{\mathrm{e}} + \boldsymbol{B}_{\mathrm{e}}\boldsymbol{u}_{\mathrm{e}} \end{cases} \tag{6}$$

where the states of the two players are depicted as: $\boldsymbol{\rho}_{\mathrm{p}} = \left[\boldsymbol{x}_{\mathrm{p}}^{\mathrm{T}}, \boldsymbol{v}_{\mathrm{p}}^{\mathrm{T}}\right]^{\mathrm{T}}$ and $\boldsymbol{\rho}_{\mathrm{e}} = \left[\boldsymbol{x}_{\mathrm{e}}^{\mathrm{T}}, \boldsymbol{v}_{\mathrm{e}}^{\mathrm{T}}\right]^{\mathrm{T}}$. $\boldsymbol{u}_{\mathrm{p}}$ and $\boldsymbol{u}_{\mathrm{e}}$ are the desired control forces of the pursuer and the evader. $\boldsymbol{A}$ and $\boldsymbol{B}$ are dynamic functions of player. On the one hand, considering that the forces the MUs can produce are limited, the following inequality constraints are formulated:

$$-u_{\max}\mathbf{1}_3 \leqslant \boldsymbol{u}_{\mathrm{p}} \leqslant u_{\max}\mathbf{1}_3 \tag{7}$$

where $u_{\max}$ is the maximum force that a MU can produce in one direction, $\mathbf{1}_n$ denotes a n-dimensional vector with all elements equal to one. Define the relative state between the two players as $\boldsymbol{\rho}_{\mathrm{pe}} = \boldsymbol{\rho}_{\mathrm{p}} - \boldsymbol{\rho}_{\mathrm{e}}$, the relative dynamics can be written as:

$$\dot{\boldsymbol{\rho}}_{\mathrm{pe}} = \boldsymbol{A}_{\mathrm{pe}}\boldsymbol{\rho}_{\mathrm{pe}} + \boldsymbol{B}_{\mathrm{p}}\boldsymbol{u}_{\mathrm{p}} - \boldsymbol{B}_{\mathrm{e}}\boldsymbol{u}_{\mathrm{e}} \tag{8}$$

In the pursuit-evasion game, the goal of the pursuer is to intercept the evader at the minimum cost. Conversely, the evader has the goal to increase the relative distance at the minimum cost. The cost function can be expressed as:

$$\min_{\boldsymbol{u}_{\mathrm{p}}} \max_{\boldsymbol{u}_{\mathrm{e}}} J = \frac{1}{2}\boldsymbol{\rho}_{\mathrm{pe}}^{\mathrm{T}}(t_{\mathrm{f}})\boldsymbol{S}\boldsymbol{\rho}_{\mathrm{pe}}(t_{\mathrm{f}}) + \frac{1}{2}\int_{t_0}^{t_{\mathrm{f}}} \left(\boldsymbol{\rho}_{\mathrm{pe}}^{\mathrm{T}}\boldsymbol{Q}\boldsymbol{\rho}_{\mathrm{pe}} + \boldsymbol{u}_{\mathrm{p}}^{\mathrm{T}}\boldsymbol{R}_{\mathrm{p}}\boldsymbol{u}_{\mathrm{p}} - \boldsymbol{u}_{\mathrm{e}}^{\mathrm{T}}\boldsymbol{R}_{\mathrm{e}}\boldsymbol{u}_{\mathrm{e}}\right)\mathrm{d}t \tag{9}$$

where t_0 is the initial time, t_{f} is the terminal time, $\boldsymbol{S} > \boldsymbol{0}$, $\boldsymbol{R}_{\mathrm{p}} > \boldsymbol{0}$, and $\boldsymbol{R}_{\mathrm{e}} > \boldsymbol{0}$ are symmetric positive definite matrices, $\boldsymbol{Q} \geqslant \boldsymbol{0}$ is a semidefinite symmetric positive matrix. The cost

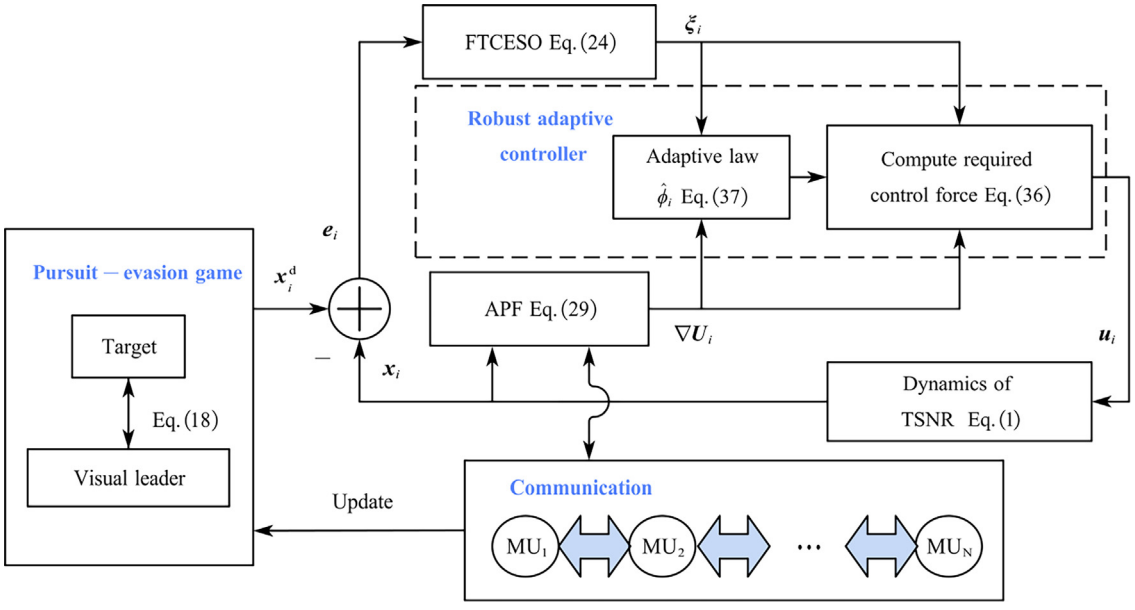

Fig. 3 Schematic flowchart of the proposed control scheme.

function comprises three components, the first part $\boldsymbol{\rho}_{\mathrm{pe}}^{\mathrm{T}}(t_{\mathrm{f}})\boldsymbol{S}\boldsymbol{\rho}_{\mathrm{pe}}(t_{\mathrm{f}})$ is the terminal conditions, reflecting the pursuit at the moment of termination. The second part $\boldsymbol{\rho}_{\mathrm{pe}}^{\mathrm{T}}\boldsymbol{Q}\boldsymbol{\rho}_{\mathrm{pe}}$ represents the relative distance between the two players at each moment, guiding the optimization of the cost function. The third component $\boldsymbol{u}_{\mathrm{p}}^{\mathrm{T}}\boldsymbol{R}_{\mathrm{p}}\boldsymbol{u}_{\mathrm{p}}-\boldsymbol{u}_{\mathrm{e}}^{\mathrm{T}}\boldsymbol{R}_{\mathrm{e}}\boldsymbol{u}_{\mathrm{e}}$ focuses on the control inputs exerted by each player, exhibiting an inverse relationship due to the adversarial nature of the pursuit-evasion game. Throughout the chase, the pursuer aims to minimize this cost function, while the escaper seeks to maximize it.

Remark 2. In cost function Eq. (9), relative state $\boldsymbol{\rho}_{\mathrm{pe}}$, parametric $\boldsymbol{R}_{\mathrm{e}}$, and control strategy $\boldsymbol{u}_{\mathrm{e}}$ can be obtained by sensor estimations Refs. 3,31. In the game solving process of this paper, it is assumed that the above quantities have been obtained.

If both players in the game have complete information about the opponent, the game is zero-sum and associated with a saddle-point strategy pair. To derive the saddle-point strategy pair, a Hamiltonian function H and a function of terminal condition Φ are introduced as:

$$\begin{cases} H=\boldsymbol{\lambda}^{\mathrm{T}}\left(\boldsymbol{A}_{\mathrm{pe}}\boldsymbol{\rho}_{\mathrm{pe}}+\boldsymbol{B}_{\mathrm{p}}\boldsymbol{u}_{\mathrm{p}}-\boldsymbol{B}_{\mathrm{e}}\boldsymbol{u}_{\mathrm{e}}\right)+\frac{1}{2}\left(\boldsymbol{\rho}_{\mathrm{pe}}^{\mathrm{T}}\boldsymbol{Q}\boldsymbol{\rho}_{\mathrm{pe}}+\boldsymbol{u}_{\mathrm{p}}^{\mathrm{T}}\boldsymbol{R}_{\mathrm{p}}\boldsymbol{u}_{\mathrm{p}}-\boldsymbol{u}_{\mathrm{e}}^{\mathrm{T}}\boldsymbol{R}_{\mathrm{e}}\boldsymbol{u}_{\mathrm{e}}\right) \\ \Phi=\frac{1}{2}\boldsymbol{\rho}_{\mathrm{pe}}^{\mathrm{T}}(t_{\mathrm{f}})\boldsymbol{S}\boldsymbol{\rho}_{\mathrm{pe}}(t_{\mathrm{f}}) \end{cases} \tag{10}$$

where $\boldsymbol{\lambda}$ is an adjoint variable. The saddle-point strategy satisfies the stationarity condition $\partial H/\partial\boldsymbol{u}_{\mathrm{p}}=\boldsymbol{0}$ and $\partial H/\partial\boldsymbol{u}_{\mathrm{e}}=\boldsymbol{0}$. Thus, one has:

$$\begin{cases} \boldsymbol{u}_{\mathrm{p}}=-\boldsymbol{R}_{\mathrm{p}}^{-1}\boldsymbol{B}_{\mathrm{p}}^{\mathrm{T}}\boldsymbol{\lambda} \\ \boldsymbol{u}_{\mathrm{e}}=-\boldsymbol{R}_{\mathrm{e}}^{-1}\boldsymbol{B}_{\mathrm{e}}^{\mathrm{T}}\boldsymbol{\lambda} \end{cases} \tag{11}$$

The necessary condition for the optimal saddle-point solution includes the derivative of the adjoint variable, which is calculated as:

$$\dot{\boldsymbol{\lambda}}=-\frac{\partial H}{\partial\boldsymbol{\rho}_{\mathrm{pe}}}=-\left(\boldsymbol{A}_{\mathrm{pe}}^{\mathrm{T}}\boldsymbol{\lambda}+\boldsymbol{Q}\boldsymbol{\rho}_{\mathrm{pe}}\right) \tag{12}$$

with the terminal condition:

$$\boldsymbol{\lambda}(t_{\mathrm{f}})=\frac{\partial\Phi}{\partial\boldsymbol{\rho}_{\mathrm{pe}}(t_{\mathrm{f}})}=\boldsymbol{S}\boldsymbol{\rho}_{\mathrm{pe}}(t_{\mathrm{f}}) \tag{13}$$

Assuming that the adjoint variable and the relative state satisfy a linear feedback strategy, for any time $\forall t\in[t_0,t_{\mathrm{f}}]$, the strategy always follows the form like in Eq. (13). Define $\boldsymbol{P}$ as a symmetric positive definite matrix, one has:

$$\boldsymbol{\lambda}=\boldsymbol{P}\boldsymbol{\rho}_{\mathrm{pe}} \tag{14}$$

Substituting the relative dynamics Eqs. (8), (12) and (14), a Riccati differential equation can be obtained as follows:

$$\dot{\boldsymbol{P}}+\boldsymbol{A}_{\mathrm{pe}}^{\mathrm{T}}\boldsymbol{P}+\boldsymbol{P}\boldsymbol{A}_{\mathrm{pe}}-\boldsymbol{P}\left(\boldsymbol{B}_{\mathrm{p}}\boldsymbol{R}_{\mathrm{p}}^{-1}\boldsymbol{B}_{\mathrm{p}}^{\mathrm{T}}-\boldsymbol{B}_{\mathrm{e}}\boldsymbol{R}_{\mathrm{e}}^{-1}\boldsymbol{B}_{\mathrm{e}}^{\mathrm{T}}\right)\boldsymbol{P}+\boldsymbol{Q}=\boldsymbol{0} \tag{15}$$

while the terminal condition satisfies $\boldsymbol{P}(t_{\mathrm{f}})=\boldsymbol{S}$.

If the pursuer and the evader do not confine the pursuit-evasion game to a fixed time, but instead decide to keep the game going, the problem can be considered as a problem of differential countermeasure in the infinite time domain. Then the Riccati differential equation Eq. (15) can be reformulated as:

$$\boldsymbol{A}_{\mathrm{pe}}^{\mathrm{T}}\boldsymbol{P}+\boldsymbol{P}\boldsymbol{A}_{\mathrm{pe}}-\boldsymbol{P}\left(\boldsymbol{B}_{\mathrm{p}}\boldsymbol{R}_{\mathrm{p}}^{-1}\boldsymbol{B}_{\mathrm{p}}^{\mathrm{T}}-\boldsymbol{B}_{\mathrm{e}}\boldsymbol{R}_{\mathrm{e}}^{-1}\boldsymbol{B}_{\mathrm{e}}^{\mathrm{T}}\right)\boldsymbol{P}+\boldsymbol{Q}=\boldsymbol{0} \tag{16}$$

The cost function Eq. (9) takes the following form:

$$\min_{\boldsymbol{u}_{\mathrm{p}}}\max_{\boldsymbol{u}_{\mathrm{e}}}J=\frac{1}{2}\int_{t_0}^{t_{\mathrm{f}}}\left(\boldsymbol{\rho}_{\mathrm{pe}}^{\mathrm{T}}\boldsymbol{Q}\boldsymbol{\rho}_{\mathrm{pe}}+\boldsymbol{u}_{\mathrm{p}}^{\mathrm{T}}\boldsymbol{R}_{\mathrm{p}}\boldsymbol{u}_{\mathrm{p}}-\boldsymbol{u}_{\mathrm{e}}^{\mathrm{T}}\boldsymbol{R}_{\mathrm{e}}\boldsymbol{u}_{\mathrm{e}}\right)\mathrm{d}t \tag{17}$$

Therefore, the saddle-point strategy pair, i.e., the solution of the pursuit-evasion game is given by:

$$\begin{cases} \boldsymbol{u}_{\mathrm{p}}=-\boldsymbol{R}_{\mathrm{p}}^{-1}\boldsymbol{B}_{\mathrm{p}}^{\mathrm{T}}\boldsymbol{P}\boldsymbol{\rho}_{\mathrm{pe}} \\ \boldsymbol{u}_{\mathrm{e}}=-\boldsymbol{R}_{\mathrm{e}}^{-1}\boldsymbol{B}_{\mathrm{e}}^{\mathrm{T}}\boldsymbol{P}\boldsymbol{\rho}_{\mathrm{pe}} \end{cases} \tag{18}$$

By substituting Eq. (18) into the virtual leader's dynamics Eq. (6), the leader's trajectory $\boldsymbol{x}_0$ and velocity $\boldsymbol{v}_0$ are given by: $\boldsymbol{\rho}_0=\left[\boldsymbol{x}_0^{\mathrm{T}},\boldsymbol{v}_0^{\mathrm{T}}\right]^{\mathrm{T}}$. Let $\boldsymbol{l}_i\in\mathbb{R}^3=\left[l_i^x,l_i^y,l_i^z\right]^{\mathrm{T}}$, which represents the desired displacement of the i-th MU relative to the leader. Thus, the desired trajectory of the MUs yields the following expression:

$$\begin{cases} \boldsymbol{x}_i^{\mathrm{d}}=\boldsymbol{x}_0+\boldsymbol{l}_i \\ \boldsymbol{v}_i^{\mathrm{d}}=\boldsymbol{v}_0 \end{cases} \tag{19}$$

The desired formation pattern of the MUs is determined by the vector $\boldsymbol{l}_{ij}\in\mathbb{R}^3=\left[l_{ij}^x,l_{ij}^y,l_{ij}^z\right]^{\mathrm{T}}$, where $\boldsymbol{l}_{ij}$ denotes the desired relative position between the i-th MU and the j-th MU. Moreover, the desired relative position $\boldsymbol{l}_{ij}$ can be written as:

$$\boldsymbol{l}_{ij}=\boldsymbol{x}_i^{\mathrm{d}}-\boldsymbol{x}_j^{\mathrm{d}}=\boldsymbol{l}_i-\boldsymbol{l}_j \tag{20}$$

Remark 3. It is noteworthy that the TSNR cannot effectively track the virtual leader in the presence of external disturbances. To ensure system stability, it becomes necessary to re-plan the pursuit trajectory when the controller fails to compensate for the deviation. If the distance between the center of the TSNR and the virtual leader exceeds a maximum distance, re-plan the pursuit trajectory:

$$\|\boldsymbol{x}_0-\boldsymbol{x}_{\mathrm{center}}\|\geqslant l_{\max} \tag{21}$$

where $\boldsymbol{x}_{\mathrm{center}}$ is the position of the center of the TSNR, $l_{\max}$ is the maximum distance. Subsequently, the position of the virtual leader is reset to the center of the TSNR, and its speed is set as the average speed of the four MUs. The game then proceeds by updating the pursuer's state.

3.2. Finite-time convergent extended state observer

When tracking the generated trajectories, tracking errors inevitably exist due to external and internal disturbances. Before further designing the controller, the tracking errors and various disturbances need to be approximated by the FTCESO. The position tracking error of the i-th MU is defined as $\boldsymbol{e}_{i1}=\boldsymbol{x}_i-\boldsymbol{x}_i^{\mathrm{d}}$, and the corresponding speed tracking error is $\boldsymbol{e}_{i2}=\boldsymbol{v}_i-\boldsymbol{v}_i^{\mathrm{d}}$, the relative motion error system can be written as:

$$\begin{cases} \dot{\boldsymbol{e}}_{i1} = \boldsymbol{e}_{i2} \\ \dot{\boldsymbol{e}}_{i2} = \boldsymbol{e}_{i3} + \boldsymbol{u}_i \\ \dot{\boldsymbol{e}}_{i3} = \dot{\boldsymbol{G}}(t) \end{cases} \tag{22}$$

where $\boldsymbol{G}(t) = \boldsymbol{f}(\boldsymbol{x}_i, \boldsymbol{v}_i) + \boldsymbol{d}_i$, with assuming $\| \dot{\boldsymbol{G}}(t) \| \leqslant U_{\mathrm{f}}$.

Based on the error system Eq. (22), a FTCESO can be constructed as:

$$\begin{cases} \boldsymbol{\sigma}_{i1} = \boldsymbol{e}_{i1} - \boldsymbol{\xi}_{i1} \\ \dot{\boldsymbol{\xi}}_{i1} = \boldsymbol{\xi}_{i2} + k_1 \mathrm{sig}^{(\kappa+1)/2}(\boldsymbol{\sigma}_i) \\ \dot{\boldsymbol{\xi}}_{i2} = \boldsymbol{\xi}_{i3} + k_2 \mathrm{sig}^{(\kappa+1)/2}(\boldsymbol{\sigma}_i) + \boldsymbol{u}_i \\ \dot{\boldsymbol{\xi}}_{i3} = k_3 \mathrm{sig}^{\kappa}(\boldsymbol{\sigma}_i) \end{cases} \tag{23}$$

where $\boldsymbol{\xi}_{i1}$, $\boldsymbol{\xi}_{i2}$, and $\boldsymbol{\xi}_{i3}$ are the estimations of $\boldsymbol{e}_{i1}$, $\boldsymbol{e}_{i2}$, and $\boldsymbol{e}_{i3}$; $\kappa \in (0, 1)$; k_1, k_2, and k_3 are the observer gains; $\mathrm{sig}^h(g) = \mathrm{sign}(g)|g|^h$. In addition, define the observation error of the FTCESO as $\boldsymbol{\sigma}_{ij} = \boldsymbol{e}_{ij} - \boldsymbol{\xi}_{ij}, j \in \{1, 2, 3\}$. Define $\| \boldsymbol{\sigma}_{i3} \| \leqslant \Delta_{i1}$. Then the FTCESO has the following representation:

$$\begin{cases} \dot{\boldsymbol{\sigma}}_{i1} = \boldsymbol{\sigma}_{i2} - k_1 \mathrm{sig}^{(\kappa+1)/2}(\boldsymbol{\sigma}_{i1}) \\ \dot{\boldsymbol{\sigma}}_{i2} = \boldsymbol{\sigma}_{i3} - k_2 \mathrm{sig}^{(\kappa+1)/2}(\boldsymbol{\sigma}_{i1}) \\ \dot{\boldsymbol{\sigma}}_{i3} = -\dot{\boldsymbol{e}}_{i3} - k_3 \mathrm{sig}^{\kappa}(\boldsymbol{\sigma}_{i1}) \end{cases} \tag{24}$$

Remark 4. According to Ref. 20, with the assumption that $\| \dot{\boldsymbol{G}}(t) \| \leqslant U_{\mathrm{f}}$, the observation error can converge within a finite time t_{s}, by appropriately choosing the observer gains k_1, k_2, and k_3. The observation error in one direction $\boldsymbol{\sigma} = \left[\mathrm{sig}^{(\kappa+1)/2}(\sigma_1), \quad \sigma_2, \quad \sigma_3 \right]^{\mathrm{T}}$ satisfies the following inequality:

$$\| \boldsymbol{\sigma} \| \leqslant \frac{l U_{\mathrm{f}}}{\sigma_{\min}\{\boldsymbol{M}\} \cdot \sigma_{\min}\{\boldsymbol{N}\}} = \sigma_{\mathrm{f}}, \forall t > t_{\mathrm{s}} \tag{25}$$

where $\sigma_{\min}(\boldsymbol{K})$ represents the minimum singular value of the matrix $\boldsymbol{K}$. The constant $l = \sqrt{k_3^2 + 4}$, the σ_{f} is the terminal error, and the matrices are:

$$\begin{cases} \boldsymbol{M} = \begin{bmatrix} k_1 & -1 & 0 \\ k_2 & 0 & -1 \\ k_3 & 0 & 0 \end{bmatrix} \\ \boldsymbol{N} = \begin{bmatrix} 2k_1/(\kappa+1) + k_2^2 + k_3^2 & -k_2 & -k_3 \\ -k_2 & 2 & 0 \\ -k_3 & 0 & 2 \end{bmatrix} \end{cases} \tag{26}$$

The convergence time t_{s}, depending on the initial error $\boldsymbol{\sigma}_0$, can be obtained as:

$$t_{\mathrm{s}} \leqslant \frac{2(m+n)}{mn} \left(\lambda_{\max}\{\boldsymbol{N}\} V(\boldsymbol{\sigma}_0) \right)^{1/2} \tag{27}$$

The expressions of α, β, V are:

$$\begin{cases} m = (\kappa+1)\sigma_{\min}\{\boldsymbol{M}\}\sigma_{\min}\{\boldsymbol{N}\} - 2lU_{\mathrm{f}} \\ n = 2\sigma_{\mathrm{f}}\sigma_{\min}\{\boldsymbol{M}\}\sigma_{\min}\{\boldsymbol{N}\} - 2lU_{\mathrm{f}} \\ V = \boldsymbol{\sigma}^{\mathrm{T}}\boldsymbol{N}\boldsymbol{\sigma} \end{cases} \tag{28}$$

3.3. Artificial potential field

When tracking the trajectory, the excessive relative distance between the MUs will create a large force that will cause the TSNR instability, and too close can lead to collision and entanglement. In order to guarantee the relative distance requirements in Eq. (2), two parts of the artificial potential function are designed as:

$$U(\boldsymbol{x}, \boldsymbol{x}^{\mathrm{d}}) = \sum_{i=1}^{\mathrm{N}} U_i^{\mathrm{t}}(\| \boldsymbol{x}_i - \boldsymbol{x}_i^{\mathrm{d}} \|) + \sum_{i=1}^{\mathrm{N}-1} \sum_{j \in \boldsymbol{\Omega}_i}^{j>i} U_{ij}(\| \boldsymbol{x}_i - \boldsymbol{x}_j \|) \tag{29}$$

where $\boldsymbol{x} = \left[\boldsymbol{x}_1^{\mathrm{T}}, \boldsymbol{x}_2^{\mathrm{T}}, \cdots, \boldsymbol{x}_N^{\mathrm{T}} \right]^{\mathrm{T}}$, and $\boldsymbol{x}^{\mathrm{d}} = \left[\boldsymbol{x}_1^{\mathrm{d}\,\mathrm{T}}, \boldsymbol{x}_2^{\mathrm{d}\,\mathrm{T}}, \cdots, \boldsymbol{x}_{\mathrm{N}}^{\mathrm{d}\,\mathrm{T}} \right]^{\mathrm{T}}$ are the stack vectors. The first part $U_i^{\mathrm{t}}(\| \boldsymbol{x}_i - \boldsymbol{x}_i^{\mathrm{d}} \|)$ is a gravitational field with the desired trajectory $\boldsymbol{x}_i^{\mathrm{d}}$ as the gravitational point. It keeps the i-th MU tracking its own trajectory. The second part $U_{ij}(\| \boldsymbol{x}_i - \boldsymbol{x}_j \|)$ is a repulsive field, including the minimum safety distance ℓ_0 and maximum allowable distance $L_{ij} + \delta$ two repulsive points. U_{ij} is used to satisfy the relative distance constraints between the MUs, and maintain the desired formation.

$$U_i^{\mathrm{t}}(\| \boldsymbol{x}_i - \boldsymbol{x}_i^{\mathrm{d}} \|) = \| \boldsymbol{x}_i - \boldsymbol{x}_i^{\mathrm{d}} \| \tag{30}$$

It always satisfies $U_i^{\mathrm{t}}(\| \boldsymbol{x}_i - \boldsymbol{x}_i^{\mathrm{d}} \|) > 0$, and equal to 0 when $\boldsymbol{x}_i = \boldsymbol{x}_i^{\mathrm{d}}$.

$$U_{ij}(\| \boldsymbol{x}_i - \boldsymbol{x}_j \|) = \begin{cases} \dfrac{1}{\sin\left(\frac{\pi \| \boldsymbol{x}_i - \boldsymbol{x}_j \|}{2\left(L_{ij}+\delta-l_{ij}\right)} - \frac{\pi\left(l_{ij} - \left(L_{ij}+\delta-l_{ij}\right)\right)}{2\left(L_{ij}+\delta-l_{ij}\right)} \right)}, l_{ij} < \| \boldsymbol{x}_i - \boldsymbol{x}_j \| < L_{ij} + \delta \\ \dfrac{1}{\sin\left(\frac{\pi \| \boldsymbol{x}_i - \boldsymbol{x}_j \|}{2\left(l_{ij}-\ell_0\right)} - \frac{\pi \ell_0}{2\left(l_{ij}-\ell_0\right)} \right)}, \ell_0 < \| \boldsymbol{x}_i - \boldsymbol{x}_j \| \leqslant l_{ij} \\ 0, \text{ others} \end{cases} \tag{31}$$

If $\| \boldsymbol{x}_i - \boldsymbol{x}_i^{\mathrm{d}} \| \to \ell_0$ or $\| \boldsymbol{x}_i - \boldsymbol{x}_i^{\mathrm{d}} \| \to L_{ij} + \delta$, $U_{ij}(\| \boldsymbol{x}_i - \boldsymbol{x}_j \|) \to \infty$. The function $U_{ij}(\| \boldsymbol{x}_i - \boldsymbol{x}_j \|)$ takes the local minimum at $\| \boldsymbol{x}_i - \boldsymbol{x}_i^{\mathrm{d}} \| = l_{ij}$.

According to Ref. 8, the partial derivatives of the potential function with respect to $\boldsymbol{x}_i$ and $\boldsymbol{x}_i^{\mathrm{d}}$, $\nabla_{\boldsymbol{x}_i} U(\boldsymbol{x}, \boldsymbol{x}^{\mathrm{d}})$ and $\nabla_{\boldsymbol{x}_i^{\mathrm{d}}} U(\boldsymbol{x}, \boldsymbol{x}^{\mathrm{d}})$ have the following relationships:

$$\sum_{i=1}^{N} \nabla_{\boldsymbol{x}_i^{\mathrm{d}}} U(\boldsymbol{x}, \boldsymbol{x}^{\mathrm{d}}) = -\sum_{i=1}^{N} \nabla_{\boldsymbol{x}_i} U(\boldsymbol{x}, \boldsymbol{x}^{\mathrm{d}}) \tag{32}$$

Then, the derivative of $U(\boldsymbol{x}, \boldsymbol{x}^{\mathrm{d}})$ can be expressed as:

$$\begin{aligned} \dot{U}(\boldsymbol{x}, \boldsymbol{x}^{\mathrm{d}}) &= \sum_{i=1}^{N} \nabla_{\boldsymbol{x}_i} U^{\mathrm{T}}(\boldsymbol{x}, \boldsymbol{x}^{\mathrm{d}}) \dot{\boldsymbol{x}}_i + \sum_{i=1}^{N} \nabla_{\boldsymbol{x}_i^{\mathrm{d}}} U^{\mathrm{T}}(\boldsymbol{x}, \boldsymbol{x}^{\mathrm{d}}) \dot{\boldsymbol{x}}_i^{\mathrm{d}} \\ &= \sum_{i=1}^{N} \nabla_{\boldsymbol{x}_i} U^{\mathrm{T}}(\boldsymbol{x}, \boldsymbol{x}^{\mathrm{d}}) \boldsymbol{e}_{i2} \end{aligned} \tag{33}$$

The above equation will be used to prove the stability of the controller in Section 3.4.

Remark 5. When the gravitational potential fields $U_i^{\mathrm{t}}(\| \boldsymbol{x}_i - \boldsymbol{x}_i^{\mathrm{d}} \|)$ and repulsive potential fields $U_{ij}(\| \boldsymbol{x}_i - \boldsymbol{x}_j \|)$ cancel each other, the MU reaches the local minimum point, and the gradient $\nabla_{\boldsymbol{x}_i} U(\boldsymbol{x}, \boldsymbol{x}^{\mathrm{d}})$ is zero. Unlike classic scenarios where obstacles and targets are fixed, the gravitational point $\boldsymbol{x}_i^{\mathrm{d}}$

is momentarily changing in this paper, so the MU can easily jump out of the local minimum trap.

3.4. Robust adaptive controller

To accurately maintain the configuration of the TSNR, A robust adaptive controller is proposed based on the FTCESO and the APF designed before. To design the controller of the MUs, introduce the following sliding variable:

$$\boldsymbol{s}_i = \boldsymbol{e}_{i2} + \beta_{1i}\boldsymbol{e}_{i1} + \alpha\nabla_{\boldsymbol{x}_i}U(\boldsymbol{x},\boldsymbol{x}^{\mathrm{d}}) \tag{34}$$

where β_{1i} and α are the positive constants. The derivative of $\boldsymbol{s}_i$ is calculated as:

$$\dot{\boldsymbol{s}}_i = \dot{\boldsymbol{e}}_{i2} + \beta_{1i}\dot{\boldsymbol{e}}_{i1} + \alpha\frac{\mathrm{d}(\nabla_{\boldsymbol{x}_i}U(\boldsymbol{x},\boldsymbol{x}^{\mathrm{d}}))}{\mathrm{d}t} \tag{35}$$

Assume $\| \alpha\frac{\mathrm{d}(\nabla_{\boldsymbol{x}_i}U(\boldsymbol{x},\boldsymbol{x}^{\mathrm{d}}))}{\mathrm{d}t} \| \leqslant \Delta_{i2}$. Based on the error mode Eq. (22), game-generated trajectory Eq. (19), FTCESO Eq. (24), and nonlinear sliding model function Eq. (34), the formation controller is designed as:

$$\boldsymbol{u}_i = -\boldsymbol{\xi}_{i3} - \beta_{1i}\boldsymbol{e}_{i2} - \beta_{2i}\boldsymbol{s}_i - \beta_{3i}\boldsymbol{s}_i^r - \widehat{\phi}_i\mathrm{sign}(\boldsymbol{s}_i) \tag{36}$$

where β_{2i} and β_{3i} are positive constants, r. And $\widehat{\phi}_i$ is the estimate of the upper bound ϕ_i, which satisfies $\phi_i \geqslant \Delta_{i1} + \Delta_{i2}$. The adaptive updating law for the robustness gain $\widehat{\phi}_i$ is designed as:

$$\dot{\widehat{\phi}}_i = h_i\| \boldsymbol{s}_i \|_1 \tag{37}$$

where h_i is a positive constant, and $\| \cdot \|_1$ is the one norm of the vector. Define the estimation error as $\widetilde{\phi}_i = \phi_i - \hat{\phi}_i$.

Theorem 1. By employing the formation control scheme in Eq. (36) and Eq. (37), for systems Eq. (1) with constraints Eq. (2) , if the pursuit-evasion game can obtain a feasible trajectory Eq. (19),and the approximation error of the FTCESO Eq. (24) is bounded, then the mission of formation control can be achieved in finite time, i.e.,the MUs can track the desired formation trajectory with the desired formation pattern in finite time T_{f},and finally capture the target.

Proof. Choose a Lyapunov function candidate as:

$$V(t) = \frac{1}{2}\sum_{i=1}^{N}\boldsymbol{s}_i^{\mathrm{T}}\boldsymbol{s}_i + \frac{1}{2}\sum_{i=1}^{N}\frac{1}{h_i}\widetilde{\phi}_i^2 \tag{38}$$

Substituting Eqs. (22), (24), (35), (36), and (37) into Eq. (38) yields the following expression:

$$\begin{aligned}
\dot{V}(t) &= \sum_{i=1}^{N}\boldsymbol{s}_i^{\mathrm{T}}\dot{\boldsymbol{s}}_i - \sum_{i=1}^{N}\tfrac{1}{h_i}\widetilde{\phi}_i\dot{\hat{\phi}}_i \\
&= \sum_{i=1}^{N}\boldsymbol{s}_i^{\mathrm{T}}\left(\dot{\boldsymbol{e}}_{i2} + \beta_{1i}\dot{\boldsymbol{e}}_{i1} + \alpha\tfrac{\mathrm{d}\nabla_{\boldsymbol{x}_i}U(\boldsymbol{x},\boldsymbol{x}^{\mathrm{d}})}{\mathrm{d}t}\right) - \sum_{i=1}^{N}\tfrac{1}{h_i}\widetilde{\phi}_i\dot{\hat{\phi}}_i \\
&= \sum_{i=1}^{N}\boldsymbol{s}_i^{\mathrm{T}}\left(\boldsymbol{e}_{i3} + \beta_{1i}\boldsymbol{e}_{i2} + \alpha\tfrac{\mathrm{d}\nabla_{\boldsymbol{x}_i}U(\boldsymbol{x},\boldsymbol{x}^{\mathrm{d}})}{\mathrm{d}t} - \boldsymbol{\xi}_{i3} - \beta_{1i}\boldsymbol{e}_{i2} - \dot{\hat{\phi}}_i\mathrm{sign}(\boldsymbol{s}_i) - \beta_{2i}\boldsymbol{s}_i - \beta_{3i}\boldsymbol{s}_i^r\right) - \sum_{i=1}^{N}\tfrac{1}{h_i}\widetilde{\phi}_i\dot{\hat{\phi}}_i \\
&\leqslant \sum_{i=1}^{N}\boldsymbol{s}_i^{\mathrm{T}}\left(\Delta_{i1} + \Delta_{i2} - \dot{\hat{\phi}}_i\mathrm{sign}(\boldsymbol{s}_i) - \beta_{2i}\boldsymbol{s}_i - \beta_{3i}\boldsymbol{s}_i^r\right) - \sum_{i=1}^{N}\tfrac{1}{h_i}\widetilde{\phi}_i\dot{\hat{\phi}}_i
\end{aligned} \tag{39}$$

The following inequality holds:

$$\begin{aligned}
\boldsymbol{s}_i^{\mathrm{T}}(\Delta_{i1} + \Delta_{i2}) &\leqslant \| \boldsymbol{s}_i^{\mathrm{T}}\Delta_{i1} \|_1 + \| \boldsymbol{s}_i^{\mathrm{T}}\Delta_{i2} \|_1 \\
&\leqslant \| \boldsymbol{s}_i \|_1\| \Delta_{i1} \|_1 + \| \boldsymbol{s}_i \|_1\| \Delta_{i2} \|_1 \\
&\leqslant \phi_i\| \boldsymbol{s}_i \|_1
\end{aligned} \tag{40}$$

Therefore, Eq. (39) reduces to:

$$\dot{V}(t) \leqslant -\sum_{i=1}^{N}\boldsymbol{s}_i^{\mathrm{T}}\beta_{2i}\boldsymbol{s}_i - \sum_{i=1}^{N}\boldsymbol{s}_i^{\mathrm{T}}\beta_{3i}\boldsymbol{s}_i^r \tag{41}$$

According to Lemma 1, Eq. (41) can be calculated as:

$$\dot{V}(t) \leqslant -\lambda_{\min}(\boldsymbol{\beta}_2)\sum_{i=1}^{N}\boldsymbol{s}_i^{\mathrm{T}}\boldsymbol{s}_i - \lambda_{\min}(\boldsymbol{\beta}_3)\sum_{i=1}^{N}\left(\boldsymbol{s}_i^{\mathrm{T}}\boldsymbol{s}_i\right)^{(r+1)/2} \tag{42}$$

where $\boldsymbol{\beta}_2$ and $\boldsymbol{\beta}_3$ are diagonal matrices composed of β_{2i} and β_{3i}, respectively.

Then one has:

$$\begin{aligned}
\dot{V}(t) &\leqslant -p\sum_{i=1}^{N}V_i - q\sum_{i=1}^{N}V_i^{(r+1)/2} \\
&\leqslant -pV - qV^{(r+1)/2}
\end{aligned} \tag{43}$$

where $p = \lambda_{\min}(\boldsymbol{\beta}_2)$, and $q = \lambda_{\min}(\boldsymbol{\beta}_3)$. According to Lemma 2 and Eq. (43), when $p > 0$ and $q > 0$, the system can achieve finite-time stability. Theorem 1 is proven. And the convergence time T_{f} can be obtained as:

$$T_{\mathrm{f}} \leqslant t_0 + \frac{1}{p(1-r)/2}\ln\frac{pV^{(1-r)/2}(\boldsymbol{x}_0) + q}{q} \tag{44}$$

Remark 6. The convergence time t_{s} of the FCTESO given by Eq. (27) must be faster than the convergence time T_{f} of the controller in Eq. (44).

Remark 7. It is obvious that $V(t)$ is bounded and $\dot{V}(t) \leqslant 0$ for $\forall t \geqslant 0$, which further indicates that both $\boldsymbol{s}_i$ and $\widetilde{\phi}_i$ are bounded. According to the definition of $\boldsymbol{s}_i$ in Eq. (34), $\boldsymbol{e}_{i1}$, $\boldsymbol{e}_{i2}$, and $\nabla_{\boldsymbol{x}_i}U(\boldsymbol{x},\boldsymbol{x}^{\mathrm{d}})$ are bounded. Then the relative distance constraints Eq. (2) can be guaranteed all the time.

Furthermore, $\dot{U}(\boldsymbol{x},\boldsymbol{x}^{\mathrm{d}}) = \sum_{i=1}^{N}\nabla_{\boldsymbol{x}_i}U^{\mathrm{T}}(\boldsymbol{x},\boldsymbol{x}^{\mathrm{d}})\boldsymbol{e}_{i2}$, $\dot{U}(\boldsymbol{x},\boldsymbol{x}^{\mathrm{d}})$ is also bounded. Integrating both sides of Eq. (33) over the time interval $[0\infty)$, one has:

$$\begin{aligned}
\int_{t=0}^{\infty}\dot{U}(\boldsymbol{x},\boldsymbol{x}^{\mathrm{d}})\mathrm{d}t &= \sum_{i=1}^{N}\int_{t=0}^{\infty}\left(\nabla_{\boldsymbol{x}_i}U(\boldsymbol{x},\boldsymbol{x}^{\mathrm{d}})^{\mathrm{T}}\boldsymbol{e}_{i2}\right)\mathrm{d}t \\
&= U(\boldsymbol{x},\boldsymbol{x}^{\mathrm{d}})\big|_{t=\infty} - U(\boldsymbol{x},\boldsymbol{x}^{\mathrm{d}})\big|_{t=0} \\
&< \infty
\end{aligned} \tag{45}$$

Obviously, $\int_{t=0}^{\infty}\left(\nabla_{\boldsymbol{x}_i}U(\boldsymbol{x},\boldsymbol{x}^{\mathrm{d}})^{\mathrm{T}}\boldsymbol{e}_{i2}\right)\mathrm{d}t$ exist and bounded, and $\lim_{t\to\infty}\nabla_{\boldsymbol{x}_i}U(\boldsymbol{x},\boldsymbol{x}^{\mathrm{d}}) = 0$, which indicates that the MUs can maintain the desired formation pattern.

Remark 8. Integrating both sides of Eq. (41) over the time interval $[0\infty)$, one has:

$$\begin{aligned}
\int_{t=0}^{\infty}\left(\sum_{i=1}^{N}\boldsymbol{s}_i^{\mathrm{T}}\beta_{2i}\boldsymbol{s}_i + \sum_{i=1}^{N}\boldsymbol{s}_i^{\mathrm{T}}\beta_{3i}\boldsymbol{s}_i^r\right)\mathrm{d}t &\leqslant -\int_{t=0}^{\infty}\dot{V}(t)\mathrm{d}t \\
&= V(0) - V(\infty)
\end{aligned} \tag{46}$$

Then, $s_i \in L_2$, and $\lim_{t\to\infty} s_i(t) = 0$. By Eq. (36), the conclusion can be obtained as:

$$\lim_{t\to\infty}(e_{i2} + \beta_{1i}e_{i1}) = \lim_{t\to\infty}\left(s_i - \nabla_{x_i}U(x, x^{\mathrm{d}})\right) = 0 \tag{47}$$

Therefore, $x_i \to x_i^{\mathrm{d}}$ and $\dot{x}_i \to \dot{x}_i^{\mathrm{d}}$, which implies the MUs can track the desired formation trajectory.

3.5. Discussion

Although the pursuit-evasion game in Section 3.1 is also an optimization process, it is different from the classic cooperative formation control problem, like in Ref. 18. In cooperative tasks, all agents share a common objective of reaching the specific target location with the desired formation pattern, and energy optimization involves minimizing the whole energy assumption of all agents. Conversely, the players' objectives differ in non-cooperative scenarios like the pursuit-evasion game, as described in Eq. (9). The TSNR aims to catch up with the target as quickly as possible with the minimum fuel, while the target seeks to get out of the chase with the minimum fuel, which is reflected in the cost function Eq. (9) by minimizing it on one side and maximizing it on the other side.

The energy cost $u_{\mathrm{p}}^{\mathrm{T}}R_{\mathrm{p}}u_{\mathrm{p}} - u_{\mathrm{e}}^{\mathrm{T}}R_{\mathrm{e}}u_{\mathrm{e}}$ is a significant component in the cost function. Different from the energy E in Ref. 18 is the sum of all agents, an increase in the TSNR's control input leads to an increase in its own cost function, but an increase in the target control input leads to a decrease in it. The TSNR minimizes its own energy cost while maximizing the target's fuel consumption, reflecting the adversarial nature of the pursuit-evasion game.

In addition to energy consumption, relative distance ρ_{pe} is also a vital factor to be focused on, $\rho_{\mathrm{pe}}^{\mathrm{T}}(t_{\mathrm{f}})S\rho_{\mathrm{pe}}(t_{\mathrm{f}})$ and $\rho_{\mathrm{pe}}^{\mathrm{T}}Q\rho_{\mathrm{pe}}$. Unlike in Ref. 18, the time-varying formation function f_i of agent i is given. During the game, both players change the state, i.e., the relative distance ρ_{pe}, by changing their control strategies u. In summary, for non-cooperative pursuit-evasion game problem, this form of the cost function Eq. (9) is more suitable for describing the opposite objective.

4. Simulation verification

4.1. Simulation environment

The parameters of the TSNR are shown in Ref. 5. Select a moment when the TSNR has been released and the initial positions of the MUs in the orbital frame are shown in Table 1.

The minimum safety distance ℓ_0 is 2 m, the side length of the net L_{ij} and the desired position between the MUs $\| l_{ij} \|$ are both 5 m, and the maximum elastic elongation is $\delta = 0.1$ m. Set the desired formation pattern as $l_1 = [0, 2.5, 2.5]^{\mathrm{T}}$, $l_2 = [0, 2.5, -2.5]^{\mathrm{T}}$, $l_3 = [0, -2.5, 2.5]^{\mathrm{T}}$, $l_4 = [0, -2.5, -2.5]^{\mathrm{T}}$. The topology graph is also shown in Ref. 8 with an adjacent matrix $G = [0,1,1,0;1,0,0,1;1,0,0,1;0,1,1,0]$. The maximum output of the thruster is 5 N.

Table 1 Initial states of MUs and virtual leader.

MU	Initial position(m)	Initial velocity(m/s)
0 (virtual leader)	$x_0 = [0,0,0]^{\mathrm{T}}$	$v_0 = [0,0,0]^{\mathrm{T}}$
1 (Aa)	$x_1 = [0,2,2]^{\mathrm{T}}$	$v_1 = [0,0,0]^{\mathrm{T}}$
2 (Ak)	$x_2 = [0,2,-2]^{\mathrm{T}}$	$v_2 = [0,0,0]^{\mathrm{T}}$
3 (Ka)	$x_3 = [0,-2,2]^{\mathrm{T}}$	$v_3 = [0,0,0]^{\mathrm{T}}$
4 (Kk)	$x_4 = [0,-2,-2]^{\mathrm{T}}$	$v_4 = [0,0,0]^{\mathrm{T}}$

For the game theory based trajectory part, assume the orbital angular velocity ω is 7.2722×10^5 rad/s. The initial position and velocity of the target are $[-1500, -500, 0]^{\mathrm{T}}$, and $[-0.1, 0, 0.01]^{\mathrm{T}}$. The maximum thrust magnitudes of the virtual leader are given by $u_{\max} = 4$ N, which is less than the maximum output of the MU's thruster. The finite time horizon is set as $t_{\mathrm{f}} = 1000$ s. The matrices in the cost function are given as follows:

$$\begin{cases} Q = \begin{bmatrix} I_3 & 0 \\ 0 & 0 \end{bmatrix} \\ R_{\mathrm{p}} = 1 \times 10^6 I_3 \\ R_{\mathrm{e}} = 2.5 \times 10^6 I_3 \end{cases}$$

The parameters of the FTCESO are $k_1 = 100, k_2 = 300$, $k_3 = 1000$. The parameters in controller are selected as $\alpha = 0.001$, $\beta_{1i} = 0.25$, $\beta_{2i} = 3$, $\beta_{3i} = 0.02$, $r = 0.2$, $h_i = 0.1$, for $i =$ Aa, Ak, Ka, Kk.

To demonstrate the effectiveness of the proposed formation control scheme, a comparison among three control methods is made:

(1) Controller 1 incorporates the proportional navigation guidance law to generate the pursuit trajectory, complemented by the robust adaptive control scheme Eq. (36) presented in this paper. The target employs the game method Eq. (18) proposed in this paper to avoid capture.
(2) Controller 2 utilizes the pursuit-evasion game approach Eq. (18) proposed in this paper, while the formation control part adopts the algorithm designed in Ref. 8.
(3) Controller 3 is based on the game method Eq. (18) and adaptive control law Eq. (36) proposed in this paper.

4.2. Criteria for successful capture

The evaluation of the capture process involves the following five critical variables: (A) The approaching error of the TSNR. (B) The position, velocity, and control input of the four MUs. (C) The configuration of the TSNR. (D) The relative distance between the four MUs. (E) The tension force.

Based on these variables, three criteria for a successful capture are established as follows: (A) A viable pursuit trajectory for the TSNR must be generated. (B) Each MU should be capable of tracking the desired trajectory. (C) The stability of the TSNR must be maintained throughout the capture process. The first criterion ensures that the target cannot escape from the TSNR. The second criterion ensures that the controller can effectively compensate for external disturbances during the pursuit process. The third criterion prevents the net from twisting or breaking. When the relative distance between the four MUs remains at the desired value, the net will maintain a state of micro-tension, which is the most stable condition.

4.3. Simulation results

Figs. 4–6 illustrate the trajectory and the configuration of the TSNR under the action of the three controllers. Three specific time points have been chosen to reflect the configuration of the TSNR. The first moment corresponds to the initial deployment, where the net is fully extended, and the relative distance between the MUs reaches its maximum. The second moment is during a maneuvering turn phase of the TSNR. The third moment represents the smooth-chasing phase. These figures demonstrate that all three controllers can effectively generate a trajectory to capture the target, with the TSNR configura-

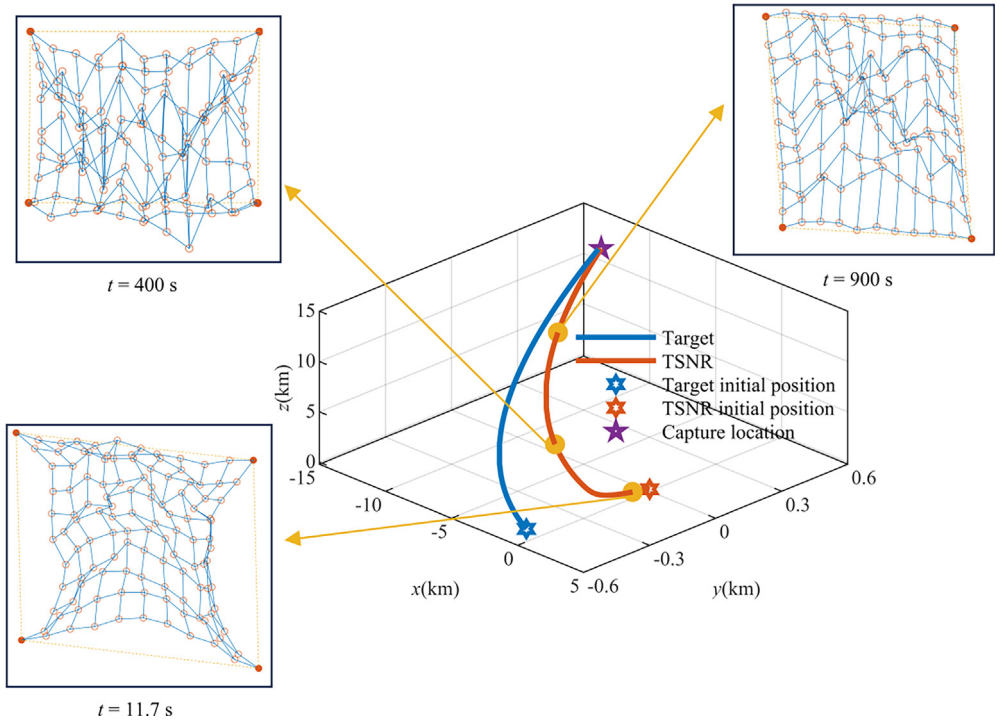

Fig. 4 Trajectory and configuration of TSNR under Controller 1.

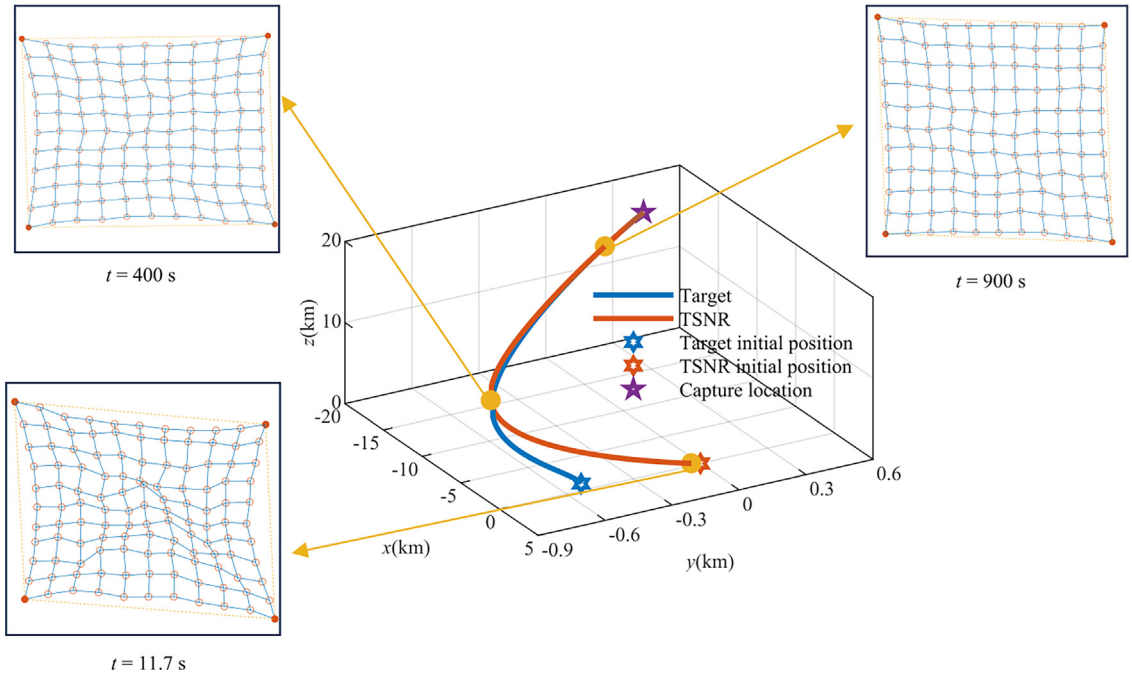

Fig. 5 Trajectory and configuration of TSNR under Controller 2.

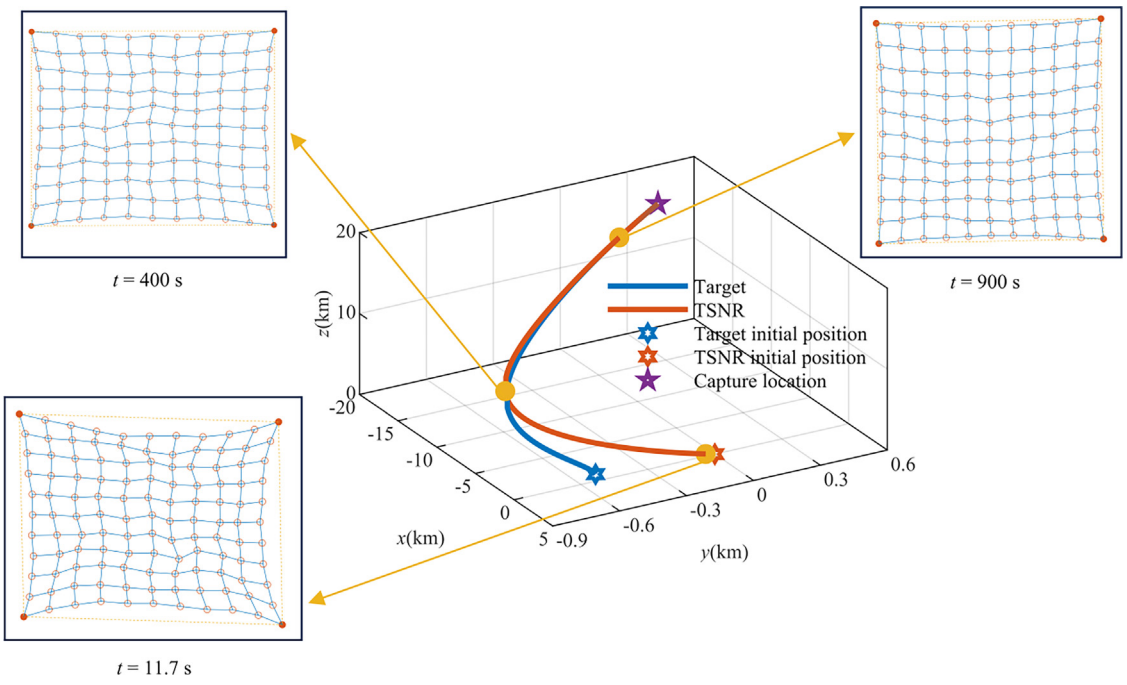

Fig. 6 Trajectory and configuration of TSNR under Controller 3.

tions displayed throughout the capture process. Upon analyzing Fig. 4, it becomes evident that Controller 1 fails to maintain the desired configuration, posing a significant threat to the system's stability. Conversely, both Controller 2 and Controller 3, which utilize the game method, not only obtain successful capture trajectories but also uphold a stable configuration consistently. Notably, in Fig. 6, the configuration at 11.7 s is more stable under the action of Controller 3 compared to controller 2, owing to the adaptive law proposed in this paper.

Fig. 7 illustrates the approaching error under the three controllers. It can be seen that the approaching error between the spacecrafts decreases rapidly. At the time horizon t_f, both Controllers 2 and 3 result in an approaching error of 1.9 m, indicating the successful conclusion of the approaching phase and the capture of the target. However, controller 1 retains an approaching error of 48 m at t_f, implying additional time to capture the target.

Fig. 8 illustrates the tension force experienced by eight nodes of the TSNR during the approaching phase. It is evident that both Controllers 2 and 3, employing the game method, result in lower tension forces compared to Controller 1. Furthermore, the inclusion of the adaptive term in Controller 3 effectively suppresses vibrations and further reduces the tension force.

Figs. 9–11 provide a comparison of the position tracking error, velocity tracking error, and control inputs for the three controllers, using MU1 (Aa) as an example. Specifically, Fig. 9 (a) and Fig. 10(a) indicate that Controller 1 fails to track the desired trajectory. This inadequate convergence accuracy leads to chaotic configurations (as shown in Fig. 4) and excessive tension force (as displayed in Fig. 8). Fig. 11(a) illustrates the high vibration of the control input, which is unacceptable for practical engineering applications. Conversely, by incorporating the game method to generate a pursuit trajectory, Controller 2 demonstrates improved tolerance and precision, as evident in Fig. 9(b) and Fig. 10(b). Consequently, this approach avoids net twisting issues (as shown in Fig. 5) and reduces tension force (as exhibited in Fig. 8). Moreover, the control input depicted in Fig. 11(b) exhibits smoother behavior, with a peak at 11.7 s attributed to the APF function. Moving on to Controller 3, Fig. 9(c) and Fig. 10(c) present the position and velocity tracking errors. Through effective compensation for disturbances caused by tension force and APF

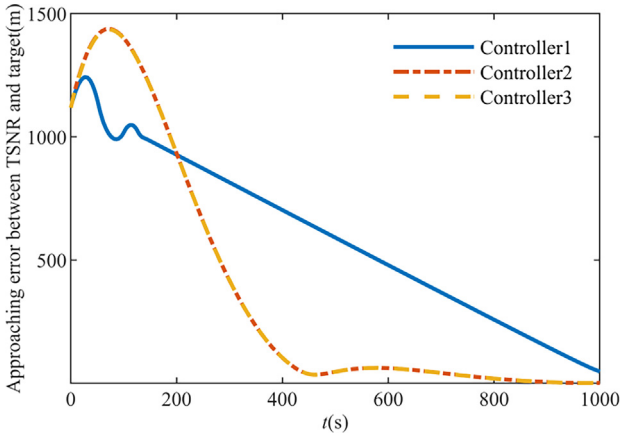

Fig. 7 Approaching error between TSNR and target.

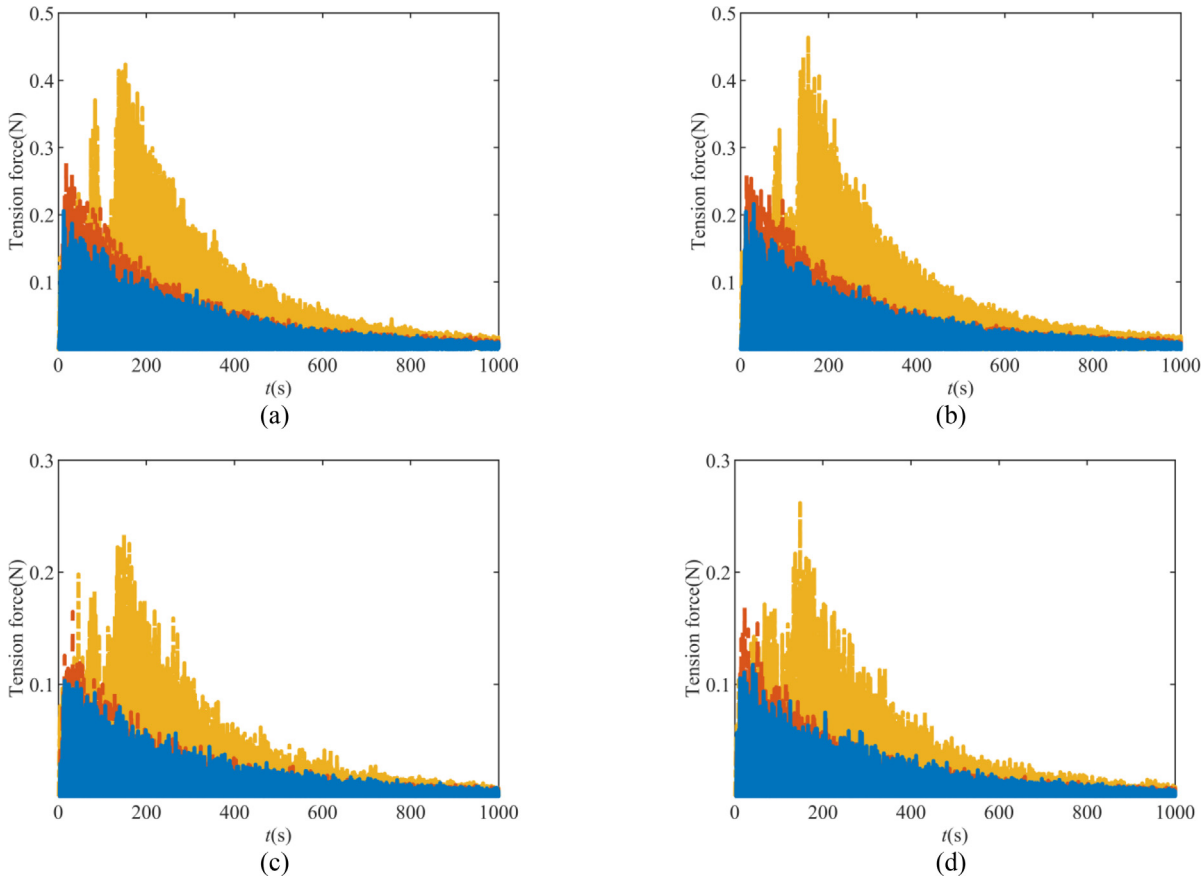

Fig. 8 Tension force of the node of TSNR. (a)Aa, (b)Ak, (c)Bc, (d)Fb, (e)Ff, (f)Ge, (g)Ka, (h)Kk.

functions, this controller successfully reduces error peaks, shortens convergence time, and improves convergence accuracy. In Fig. 11(c), the peak of the control input is lower compared to Controller 2.

The relative distances between adjacent MUs during the approaching phase, with identical initial states, are depicted in Figs. 12 to 15. It can be observed that the relative distance is strictly constrained under the three controllers due to the APF functions during the approaching phase. In the beginning, the distance is less than the predetermined value and greater than the minimum safety distance. Consequently, the APF generates a repulsive force that compels the MUs to maneuver away from each other, and the flexible net quickly becomes taut. Once the distance reaches the designed value, the attractive forces generated by the APF, along with the tension force enacted by the flexible net, affect the MUs. Moreover, when the distance is close to the maximum distance and exceeds the desired value, the APF induces a repulsive force to avoid the infringement of the constraints defined in Eq. (2), which results in the peak of the control input in Figs. 11 (b) and (c). Notably, Controller 1 does not consistently maintain the desired relative distance, resulting in extreme tension force (as demonstrated in Fig. 8) and potential system damage. On the other hand, Controllers 2 and 3 employ the pursuit-evasion game method, effectively avoiding distance oscillations and ensuring stable configurations (as evidenced in Fig. 5 and Fig. 6). However, due to the derivative of the APF function's gradient perturbing the system externally, Controller 2 exhibits slow convergence time and unsatisfactory convergence accuracy. In contrast, Controller 3 incorporates an adaptive term that compensates for this perturbation, leading to substantial improvements in convergence speed and precision. Consequently, the distances between adjacent MUs rapidly converge to the predetermined value, and the connecting net consistently maintains a state of micro-tension. In summary, Controller 3 proposed in this paper satisfies the three criteria well and outperforms the other two controllers.

5. Conclusions

This paper proposes a novel strategy to address the problems of capturing a dynamic target and maintaining a specific configuration for the TSNR. The proposed strategy combines differential game theory and formation control to efficiently accomplish the capture mission. The conclusions are drawn as follows:

(1) A pursuit-evasion game method was developed to obtain desired trajectories for approaching the target, which can evade capture. To ensure the stability of the TSNR during trajectory tracking, real-time feedback is introduced.

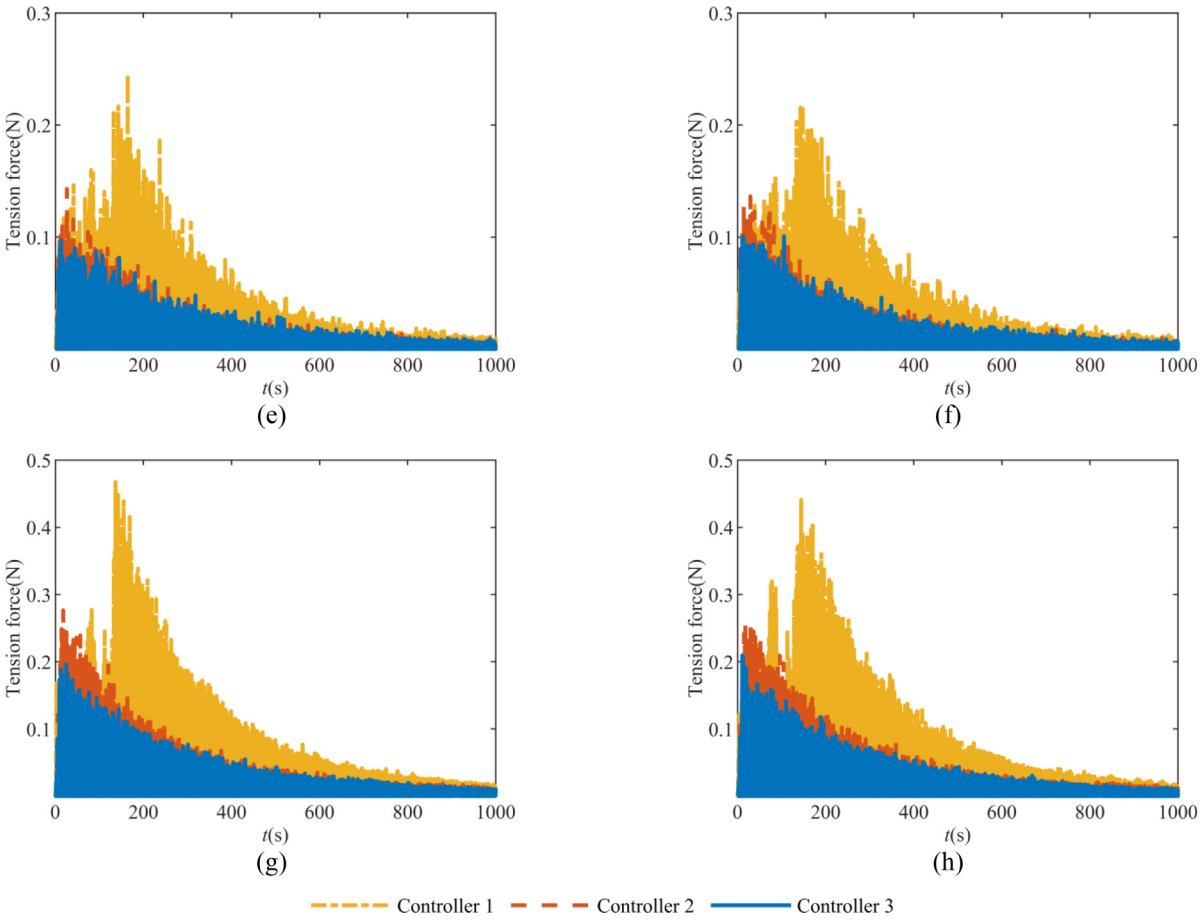

Fig. 8 (*continued*)

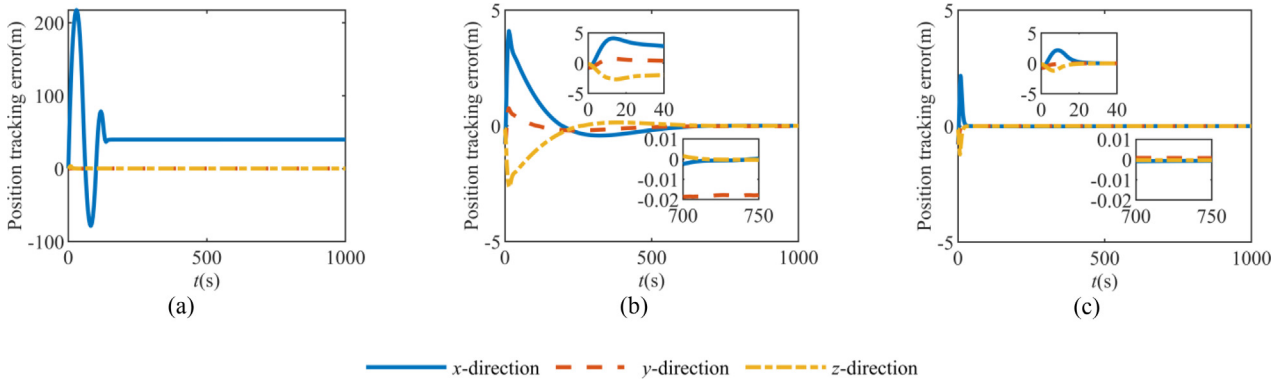

Fig. 9 Position tracking errors of MU1(Aa). (a) Under action of Controller 1. (b) Under action of Controller 2. (c) Under action of Controller 3.

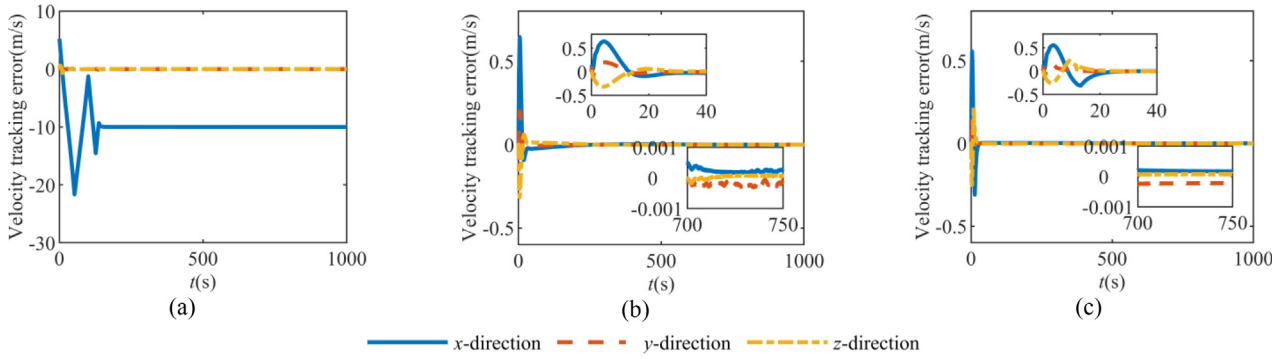

Fig. 10 Velocity tracking errors of MU1(Aa). (a) Under action of Controller 1. (b)Under action of Controller 2. (c)Under action of Controller 3.

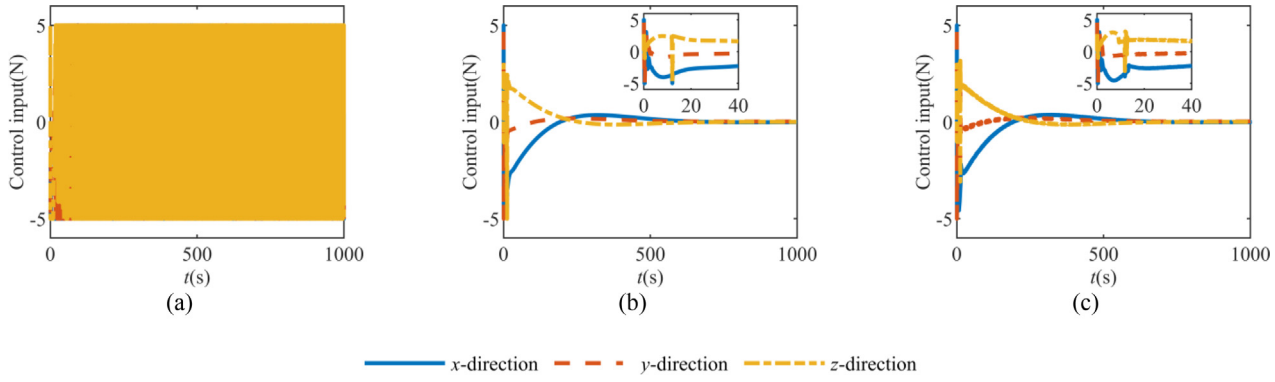

Fig. 11 Control input of MU1(Aa). (a)Under action of Controller 1. (b)Under action of Controller 2. (c)Under action of Controller 3.

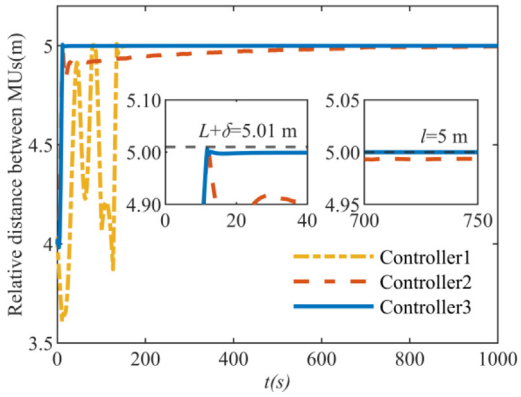

Fig. 12 Relative distance between MU1(Aa) and MU2(Ak).

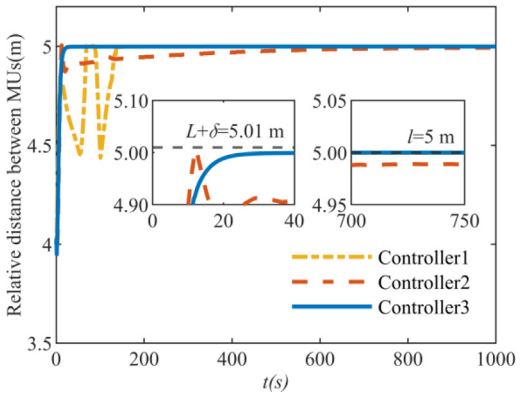

Fig. 13 Relative distance between MU1(Aa) and MU3(Ka).

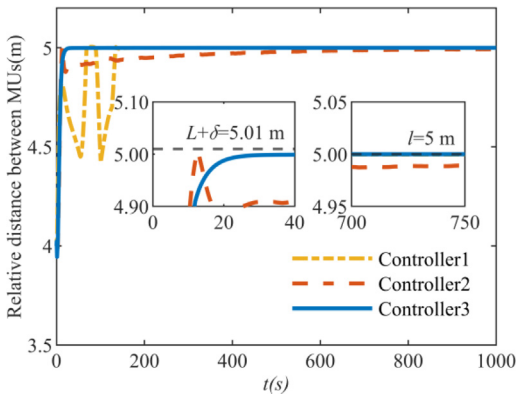

Fig. 14 Relative distance between MU2(Ak) and MU4(Kk).

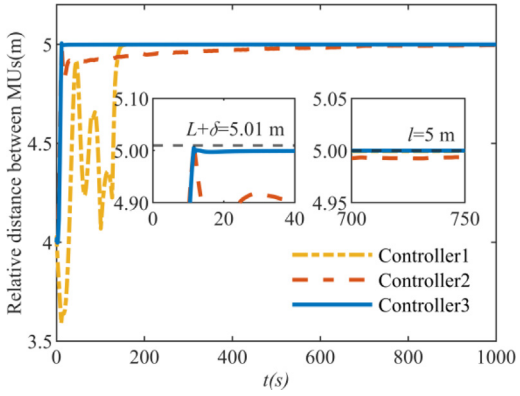

Fig. 15 Relative distance between MU3(Ka) and MU4(Kk).

(2) A formation controller with APF based on FTCESO is proposed to handle tracking errors and maintain the TSNR's configuration in the presence of disturbances. A new adaptive law is developed to estimate the derivative of the gradient of the APF functions, thus suppressing complex oscillations. Lyapunov analysis is used to verify the proposed scheme's stability and finite-time convergence.

(3) Numerical simulations demonstrate the effectiveness of the proposed strategy in capturing a dynamic target using the TSNR.

Future studies will focus on investigating the non-cooperative characteristics of the TSNR and performing a semi-physical ground test to validate the proposed method and its potential application to on-orbit scenarios.

CRediT authorship contribution statement

Yifeng MA: Conceptualization, Data curation, Methodology, Software, Visualization, Writing – original draft. **Yizhai ZHANG:** Funding acquisition, Supervision, Writing – review & editing. **Panfeng HUANG:** Funding acquisition, Supervision, Writing – review & editing. **Ya LIU:** Conceptualization, Supervision. **Fan ZHANG:** Conceptualization, Data curation, Formal analysis, Funding acquisition, Methodology, Supervision, Writing – review & editing.

Declaration of competing interest

The authors declare that they have no known competing financial interests or personal relationships that could have appeared to influence the work reported in this paper.

Acknowledgements

This study was supported by the National Natural Science Foundation of China (Nos. 62222313, 62173275, 62327809, 62303381, and 62303312), and in part by the China Postdoctoral Science Foundation (No. 2023M732225).

References

1. Shan MH, Guo J, Gill E. Review and comparison of active space debris capturing and removal methods. *Prog Aerosp Sci* 2016;**80**:18–32.
2. Benvenuto R, Salvi S, Lavagna M. Dynamics analysis and GNC design of flexible systems for space debris active removal. *Acta Astronaut* 2015;**110**:247–65.
3. Zhang YZ, Huang PF, Meng ZJ, et al. Precise angles-only navigation for noncooperative proximity operation with application to tethered space robot. *IEEE Trans Contr Syst Technol* 2019;**27**(3):1139–50.
4. Zhang F, Huang PF. Releasing dynamics and stability control of maneuverable tethered space net. *IEEE/ASME Trans Mechatron* 2017;**22**(2):983–93.
5. Zhang F, Huang PF, Meng ZJ, et al. Dynamics analysis and controller design for maneuverable tethered space net robot. *J Guid Contr Dyn* 2017;**40**(11):2828–43.
6. Ambrose RO, Aldridge H, Askew RS, et al. Robonaut: NASA's space humanoid. *IEEE Intell Syst Appl* 2000;**15**(4):57–63.
7. Sabatini M, Gasbarri P, Palmerini GB. Elastic issues and vibration reduction in a tethered deorbiting mission. *Adv Space Res* 2016;**57**(9):1951–64.
8. Liu Y, Zhang F, Huang PF. Coordinated control for constrained multiple spacecraft system. *IEEE Trans Aerosp Electron Syst* 2020;**56**(2):1189–201.
9. Zhang F, Huang PF. Fuzzy-based adaptive super-twisting sliding-mode control for a maneuverable tethered space net robot. *IEEE Trans Fuzzy Syst* 2021;**29**(7):1739–49.
10. Liu Y, Zhang F, Huang PF, et al. Fixed-time consensus tracking for second-order multiagent systems under disturbance. *IEEE Trans Syst Man Cybern Syst* 2021;**51**(8):4883–94.
11. Ye D, Shi MM, Sun ZW. Satellite proximate interception vector guidance based on differential games. *Chin J Aeronaut* 2018;**31**(6):1352–61.
12. Ye D, Shi MM, Sun ZW. Satellite proximate pursuit-evasion game with different thrust configurations. *Aerosp Sci Technol* 2020;**99**:105715.
13. Liang L, Deng F, Peng ZH, et al. A differential game for cooperative target defense. *Automatica* 2019;**102**:58–71.
14. Liang HZ, Wang JY, Liu JQ, et al. Guidance strategies for interceptor against active defense spacecraft in two-on-two engagement. *Aerosp Sci Technol* 2020;**96**:105529.
15. Chao T, Wang XT, Wang SY, et al. Linear-quadratic and norm-bounded differential game combined guidance strategy against active defense aircraft in three-player engagement. *Chin J Aeronaut* 2023;**36**(8):331–50.

16. Ning BD, Jin J, Zheng JC, et al. Finite-time and fixed-time leader-following consensus for multi-agent systems with discontinuous inherent dynamics. *Int J Contr* 2018;**91**(6):1259–70.
17. Guan ZH, Sun FL, Wang YW, et al. Finite-time consensus for leader-following second-order multi-agent networks. *IEEE Trans Circuits Syst I Regul Pap* 2012;**59**(11):2646–54.
18. Li JL, Xi JX, He M, et al. Formation control for networked multiagent systems with a minimum energy constraint. *Chin J Aeronaut* 2023;**36**(1):342–55.
19. Hua YZ, Dong XW, Han L, et al. Finite-time time-varying formation tracking for high-order multiagent systems with mismatched disturbances. *IEEE Trans Syst Man Cybern Syst* 2020;**50**(10):3795–803.
20. Zhao DJ, Yang DG. Model-free control of quad-rotor vehicle via finite-time convergent extended state observer. *Int J Contr Autom Syst* 2016;**14**(1):242–54.
21. Cai ZH, Lou J, Zhao J, et al. Quadrotor trajectory tracking and obstacle avoidance by chaotic grey wolf optimization-based active disturbance rejection control. *Mech Syst Signal Process* 2019;**128**:636–54.
22. Chen T, Wen H, Hu HY, et al. Output consensus and collision avoidance of a team of flexible spacecraft for on-orbit autonomous assembly. *Acta Astronaut* 2016;**121**:271–81.
23. Wen GX, Philip Chen CL, Liu YJ. Formation control with obstacle avoidance for a class of stochastic multiagent systems. *IEEE Trans Ind Electron* 2018;**65**(7):5847–55.
24. Li SY, Liu C, Sun ZW. Finite-time distributed hierarchical control for satellite cluster with collision avoidance. *Aerosp Sci Technol* 2021;**114**:106750.
25. Wang ZK, Xu Y, Jiang C, et al. Self-organizing control for satellite clusters using artificial potential function in terms of relative orbital elements. *Aerosp Sci Technol* 2019;**84**:799–811.
26. Wu T, Wang J, Tian BL. Periodic event-triggered formation control for multi-UAV systems with collision avoidance. *Chin J Aeronaut* 2022;**35**(8):193–203.
27. Xu Y, Wang ZK, Zhang YL. Bounded flight and collision avoidance control for satellite clusters using intersatellite flight bounds. *Aerosp Sci Technol* 2019;**94**:105425.
28. Ji J, Khajepour A, Melek WW, et al. Path planning and tracking for vehicle collision avoidance based on model predictive control with multiconstraints. *IEEE Trans Veh Technol* 2017;**66**(2):952–64.
29. Zhang Z, Wang XH, Zhang QR, et al. *Multi-robot cooperative pursuit via potential field-enhanced reinforcement learning*. Piscataway: IEEE; 2022. p. 8808–14.
30. Khoo S, Xie LH, Zhao SK, et al. Multi-surface sliding control for fast finite-time leader-follower consensus with high order SISO uncertain nonlinear agents. *Int J Robust Nonlinear Control* 2014;**24**(16):2388–404.
31. Tang X, Ye D, Huang L, et al. Pursuit-evasion game switching strategies for spacecraft with incomplete-information. *Aerosp Sci Technol* 2021;**119**:107112.